

Thermopower of gapped bilayer graphene

Lei Hao and T. K. Lee

Institute of Physics, Academia Sinica, NanKang, Taipei 11529, Taiwan

(Dated: October 29, 2018)

We calculate thermopower of clean and impure bilayer graphene systems. Opening a band gap through the application of an external electric field is shown to greatly enhance the thermopower of bilayer graphene, which is more than four times that of the monolayer graphene and gapless bilayer graphene at room temperature. The effect of scattering by dilute charged impurities is discussed in terms of the self-consistent Born approximation. Temperature dependence of the thermopower is also analyzed.

PACS numbers: 81.05.Ue, 73.50.Lw, 73.50.-h, 72.10.-d

I. INTRODUCTION

Seebeck coefficient, also called as thermopower, measures the voltage drop across a material in response to a temperature drop. The achievement of large thermopower is a prerequisite to realistic applications in heat to electric energy conversion. Thermopower, among other thermoelectric properties, also complements the conductivity in elucidating mechanisms dominating the transport processes[1]. Recently, thermopower of monolayer graphene, a peculiar two dimensional electronic system characterized by a Dirac like relativistic dispersion, attracts much attention from both experimental[2–4] and theoretical groups[1, 5–8]. Calculations taking the effect of charged impurity scattering into account could explain the experimental results very well. The experimentally observed deviation from the Mott relationship at low carrier density is interpreted in terms of electron-hole puddle formation[1] and also by mixing of valence band and conduction band states by impurity scattering[7].

Bilayer graphene is another interesting material system displaying many unusual properties. Upon applying an external voltage, a semiconducting gap is induced in the otherwise zero gap band structure[9–14]. The gap being tunable by external potential difference between the two layers introduces a new degree of freedom to bilayer graphene. Up to now, there is neither experimental nor theoretical work on thermopower of bilayer graphene. It is the purpose of this work to partially fill this gap by theoretically predicting the behavior of thermopower in bilayer graphene systems.

It is established that charged impurity scattering is primarily responsible for the transport behavior observed in monolayer graphene[15–17]. For bilayer graphene, the prediction in terms of charged impurity scattering is shown to be in qualitative agreement with the experimental result of the conductivity, and the opening of a gap in biased bilayer graphene is proposed to further improve the agreement[18]. In the present work, we theoretically study the thermopower of gapped bilayer graphene. We treat charged impurity scattering in terms of the self-consistent Born approximation (SCBA)[7, 19–21]. To ensure the applicability of SCBA, we restrict our calculations to relatively clean systems with low impu-

rity concentrations, where the localization effect is not severe[22–24]. Thermopower as a function of carrier concentration is mainly calculated at room temperature. We also study the temperature dependence of thermopower.

II. MODEL AND METHOD

We consider a bilayer graphene system composed of two graphene single layers arranged in the Bernal stacking[25]. We start from a tight binding model incorporating nearest neighboring intralayer and interlayer hopping terms. An on-site potential energy difference between the two layers is included to model the effect of an external voltage. In the presence of impurity, the Hamiltonian consists of two parts: $\hat{H} = \hat{H}_0 + \hat{H}_{imp}$. Without of magnetic field or magnetic impurities, the two spin flavors are degenerate. We ignore the spin degree of freedom here and multiply the results by two for spin dependent quantities. The free part of the Hamiltonian is then written as

$$\hat{H}_0 = \sum_{\mathbf{k}} \psi_{\mathbf{k}}^\dagger H_0(\mathbf{k}) \psi_{\mathbf{k}}, \quad (1)$$

in which the vector of fermion creation operators is defined as $\psi_{\mathbf{k}}^\dagger = (a_{1\mathbf{k}}^\dagger, b_{1\mathbf{k}}^\dagger, b_{2\mathbf{k}}^\dagger, a_{2\mathbf{k}}^\dagger)$. $a_{\alpha\mathbf{k}}^\dagger$ and $b_{\alpha\mathbf{k}}^\dagger$ create α layer states with wave vector \mathbf{k} on the A and B sublattice, respectively. Up to nearest neighbor hopping, $H_0(\mathbf{k})$ is written as[9, 25–28]

$$H_0(\mathbf{k}) = \begin{pmatrix} \frac{V}{2} & \phi(\mathbf{k}) & t_{\perp} & 0 \\ \phi^*(\mathbf{k}) & \frac{V}{2} & 0 & 0 \\ t_{\perp} & 0 & -\frac{V}{2} & \phi^*(\mathbf{k}) \\ 0 & 0 & \phi(\mathbf{k}) & -\frac{V}{2} \end{pmatrix}. \quad (2)$$

$\phi(\mathbf{k}) = -t \sum_{j=1}^3 e^{i\mathbf{k} \cdot \boldsymbol{\delta}_j}$ describes the intralayer nearest neighbor hopping with strength t . The three nearest neighbor vectors are defined as $\boldsymbol{\delta}_1 = (\frac{1}{2}, \frac{\sqrt{3}}{2})a$, $\boldsymbol{\delta}_2 = (\frac{1}{2}, -\frac{\sqrt{3}}{2})a$ and $\boldsymbol{\delta}_3 = (-1, 0)a$ [26], $a=1.42 \text{ \AA}$ is the shortest carbon-carbon bond length. t_{\perp} is the nearest-neighbor interlayer hopping energy. In this work, we take

$t=3$ eV and $t_{\perp}=0.3$ eV. V is the potential energy difference between the first and second layers induced by a bias voltage. Since for every attainable carrier density, it is possible to find a bias voltage to make the potential difference between the two layers as V (when the gap induced by V is experimentally reachable), we would not consider the Coulomb interaction between imbalanced electron densities of the two layers and also neglect the dependence of V on the carrier density n in this work[9, 10, 29–31].

For charged impurities, the impurity scattering part of the Hamiltonian is written as[7, 19, 20, 32]

$$\hat{H}_{imp} = \sum_i V_i(\mathbf{r}_i) n_i = \frac{1}{V_0} \sum_{\mathbf{q}} V_i(\mathbf{q}) \rho(\mathbf{q}). \quad (3)$$

V_0 is the volume of the system. The charge density operator is defined as $\rho(\mathbf{q}) = \sum_{\mathbf{k}} \psi_{\mathbf{k}}^{\dagger} \psi_{\mathbf{k}+\mathbf{q}}$. The electron-impurity scattering amplitude $V_i(\mathbf{q})$ could be written as $v_i(\mathbf{q}) \rho_i(-\mathbf{q})$, where $\rho_i(-\mathbf{q})$ and $v_i(\mathbf{q})$ are the Fourier components of the impurity density and the electron-impurity potential, respectively. For charged impurity, $v_i(\mathbf{q})$ is taken as of the Thomas-Fermi type[1, 7, 20]

$$v_i(\mathbf{q}) = \frac{2\pi e^2}{\epsilon(q + q_{TF})} e^{-qd}. \quad (4)$$

ϵ is the effective dielectric constant from lattice and substrate, $\epsilon=3$ is adopted in this work[7, 20, 33]. d is the distance between the impurities and the graphene plane and would be set as zero in the present work[1, 7]. q_{TF} is the Thomas-Fermi wave number and is obtained from the long-wavelength-limit static polarizability of the corresponding noninteracting electron system[1, 20] as

$$q_{TF} = 2\pi e^2 \chi / \epsilon, \quad (5)$$

with the static polarizability

$$\chi = \frac{2}{V_0} \int_0^{\beta} d\tau \langle T_{\tau} n(\tau) n^{\dagger}(0) \rangle_c. \quad (6)$$

A factor of ‘2’ comes from the two fold degeneracy in spin. The subindex ‘ c ’ means retaining only connected Feynman diagrams in evaluating the expectation value. The particle number operator is defined as

$$n(\tau) = \sum_{\mathbf{k}} \psi_{\mathbf{k}}^{\dagger}(\tau) \psi_{\mathbf{k}}(\tau) = \sum_{\mathbf{k}} \varphi_{\mathbf{k}}^{\dagger}(\tau) \varphi_{\mathbf{k}}(\tau), \quad (7)$$

where $\varphi_{\mathbf{k}}^{\dagger} = (c_{1\mathbf{k}}^{\dagger}, c_{2\mathbf{k}}^{\dagger}, c_{3\mathbf{k}}^{\dagger}, c_{4\mathbf{k}}^{\dagger})$, with $c_{\alpha\mathbf{k}}^{\dagger}$ representing the creation operator of the α -th ($\alpha=1, 2, 3, 4$) eigenstate of $H_0(\mathbf{k})$ with eigenenergy denoted as $\epsilon_{\mathbf{k}\alpha}$. Thus χ is obtained in terms of the free particle eigenstates as

$$\chi = \frac{2\beta}{V_0} \sum_{\mathbf{k}\alpha} n_F(\xi_{\mathbf{k}\alpha}) n_F(-\xi_{\mathbf{k}\alpha}), \quad (8)$$

where $\xi_{\mathbf{k}\alpha} = \epsilon_{\mathbf{k}\alpha} - \mu$ and $n_F(x) = 1/(e^{\beta x} + 1)$ is the Fermi distribution function, μ is the chemical potential. β

represents the inverse temperature $1/k_B T$, with k_B the Boltzmann constant. The value of χ and thus q_{TF} depends on both the temperature and the chemical potential.

In order to calculate the thermopower, we should first obtain the particle current and heat current operators \mathbf{j}_N and \mathbf{j}_Q . They are obtained in terms of the continuity equation, which for the particle current reads[34, 35]

$$\dot{\rho}(\mathbf{r}) + \nabla \cdot \mathbf{j}_N(\mathbf{r}) = 0. \quad (9)$$

The momentum space version of the continuity function is

$$i\dot{\rho}(\mathbf{q}) = [\rho(\mathbf{q}), \hat{H}] = \mathbf{q} \cdot \mathbf{j}_N(\mathbf{q}). \quad (10)$$

A similar relationship holds for the energy density $h_E(\mathbf{q})$ and the energy current $\mathbf{j}_E(\mathbf{q})$. With the particle density operator defined as $\rho(\mathbf{q}) = \sum_{\mathbf{k}} \sum_{\alpha=1}^2 (a_{\alpha\mathbf{k}}^{\dagger} a_{\alpha, \mathbf{k}+\mathbf{q}} + b_{\alpha\mathbf{k}}^{\dagger} b_{\alpha, \mathbf{k}+\mathbf{q}})$, the particle current operator is obtained at the $\mathbf{q}=0$ limit as

$$\mathbf{j}_N(\mathbf{q}=0) = \sum_{\mathbf{k}} \psi_{\mathbf{k}}^{\dagger} \mathbf{j}_1^{\mathbf{k}} \psi_{\mathbf{k}}, \quad (11)$$

where the matrix $\mathbf{j}_1^{\mathbf{k}}$ is defined as

$$\mathbf{j}_1^{\mathbf{k}} = \begin{pmatrix} 0 & \mathbf{v}_{\mathbf{k}} & 0 & 0 \\ \mathbf{v}_{\mathbf{k}}^* & 0 & 0 & 0 \\ 0 & 0 & 0 & \mathbf{v}_{\mathbf{k}}^* \\ 0 & 0 & \mathbf{v}_{\mathbf{k}} & 0 \end{pmatrix}, \quad (12)$$

where the velocity is defined as $\mathbf{v}_{\mathbf{k}} = \nabla_{\mathbf{k}} \phi(\mathbf{k})$. The momentum space energy density operator could be written as[36] $h_E(\mathbf{q}) = \sum_{\mathbf{k}} \psi_{\mathbf{k}}^{\dagger} h_0(\mathbf{k}, \mathbf{q}) \psi_{\mathbf{k}+\mathbf{q}} + \frac{1}{V_0} \sum_{\mathbf{q}'} V_i(\mathbf{q}') \rho(\mathbf{q}' + \mathbf{q})$, where the free part is

$$h_0(\mathbf{k}, \mathbf{q}) = \begin{pmatrix} \frac{V}{2} & \phi(\mathbf{k}, \mathbf{q}) & t_{\perp} & 0 \\ \phi^*(\mathbf{k}, \mathbf{q}) & \frac{V}{2} & 0 & 0 \\ t_{\perp} & 0 & -\frac{V}{2} & \phi^*(\mathbf{k}, \mathbf{q}) \\ 0 & 0 & \phi(\mathbf{k}, \mathbf{q}) & -\frac{V}{2} \end{pmatrix}, \quad (13)$$

where $\phi(\mathbf{k}, \mathbf{q}) = (\phi(\mathbf{k}) + \phi(\mathbf{k} + \mathbf{q}))/2$. Calculating the commutator between $h_E(\mathbf{q})$ and the Hamiltonian, the energy current operator could be obtained. The heat current operator, defined by the $\mathbf{q}=0$ limit of $\mathbf{j}_Q(\mathbf{q}) = \mathbf{j}_E(\mathbf{q}) - \mu \mathbf{j}_N(\mathbf{q})$, is written as

$$\mathbf{j}_Q(\mathbf{q}=0) = \sum_{\mathbf{k}} \psi_{\mathbf{k}}^{\dagger} \mathbf{j}_2^{\mathbf{k}} \psi_{\mathbf{k}} + \frac{1}{V_0} \sum_{\mathbf{k}, \mathbf{q}'} V_i(\mathbf{q}') \psi_{\mathbf{k}}^{\dagger} \mathbf{j}_1^{\mathbf{k}, \mathbf{q}'} \psi_{\mathbf{k}+\mathbf{q}'}, \quad (14)$$

where the free part is written as

$$\mathbf{j}_2^{\mathbf{k}} = \begin{pmatrix} \mathbf{d}(\mathbf{k}) & (\frac{V}{2} - \mu) \mathbf{v}_{\mathbf{k}} & 0 & \frac{t_{\perp}}{2} \mathbf{v}_{\mathbf{k}}^* \\ (\frac{V}{2} - \mu) \mathbf{v}_{\mathbf{k}}^* & \mathbf{d}(\mathbf{k}) & \frac{t_{\perp}}{2} \mathbf{v}_{\mathbf{k}}^* & 0 \\ 0 & \frac{t_{\perp}}{2} \mathbf{v}_{\mathbf{k}} & \mathbf{d}(\mathbf{k}) & -(\frac{V}{2} + \mu) \mathbf{v}_{\mathbf{k}}^* \\ \frac{t_{\perp}}{2} \mathbf{v}_{\mathbf{k}} & 0 & -(\frac{V}{2} + \mu) \mathbf{v}_{\mathbf{k}} & \mathbf{d}_{\mathbf{k}} \end{pmatrix}, \quad (15)$$

with $\mathbf{d}(\mathbf{k}) = \frac{1}{2}[\mathbf{v}_{\mathbf{k}}\phi^*(\mathbf{k}) + \mathbf{v}_{\mathbf{k}}^*\phi(\mathbf{k})]$. Substituting $\mathbf{v}_{\mathbf{k}}$ by $\frac{1}{2}(\mathbf{v}_{\mathbf{k}+\mathbf{q}'} + \mathbf{v}_{\mathbf{k}})$, we obtain $\mathbf{j}_1^{\mathbf{k},\mathbf{q}'}$ from $\mathbf{j}_1^{\mathbf{k}}$.

We calculate the thermopower in terms of the Kubo's formula[36, 37] with impurity scattering treated to the order of self-consistent Born approximation[7, 19, 32, 38]. The thermopower is given by[36, 39, 40]

$$S = -\frac{L_{12}}{eTL_{11}}, \quad (16)$$

where e is the absolute value of the electron charge. The linear response coefficients L_{ij} are obtained from the correlation function $\mathcal{L}_{ij}(i\omega)$ by

$$L_{ij} = \lim_{\omega \rightarrow 0} \text{Re} \mathcal{L}_{ij}(\omega + i0^+). \quad (17)$$

In the Matsubara notation, the correlation function reads[36]

$$\mathcal{L}_{ij}(i\omega_n) = -\frac{iT}{(i\omega_n)dV_0} \int_0^\beta d\tau e^{i\omega_n\tau} \langle T_\tau \mathbf{j}_i(\tau) \cdot \mathbf{j}_j(0) \rangle, \quad (18)$$

where $d = 2$ is the dimensionality, $\beta = 1/k_B T$, and T_τ indicates an ordering of the current operators with respect to the complex time τ . ω_n is the bosonic Matsubara frequency related with the current operator.

For charged impurities, only intravalley scattering is important[7, 19, 20, 41], so we neglect the intervalley scattering processes in this work. Remembering that only states close to the chemical potential contribute to the dc transport, we could focus our attention at a single valley and retain only those low energy states. Here, we would focus on the valley around $\mathbf{K} = (\sqrt{3}, 1)\frac{2\pi}{3\sqrt{3}a}$. Similar to the monolayer graphene case, this could be achieved by introducing an energy cutoff E_C , such that only when the smaller positive eigenenergy is less than E_C would the states labeled by the corresponding wave vector \mathbf{k} be retained in our calculations[7, 19]. For experimentally relevant carrier densities, E_C is no larger than 1 eV. In this energy range, $\phi(\mathbf{k}')$ could be expanded as a polynomial series in terms of the relative wave vector $\mathbf{k} = \mathbf{k}' - \mathbf{K}$. Here, we retain the expansion to the second order of \mathbf{k} as

$$\begin{aligned} \phi(\mathbf{k}) &\equiv \phi(\mathbf{k} + \mathbf{K}) = -t \sum_{j=1}^3 e^{i(\mathbf{k}+\mathbf{K}) \cdot \boldsymbol{\delta}_j} \\ &\simeq \frac{3t}{2} e^{\frac{\pi}{3}i} [k_y a - ik_x a + \frac{1}{4}(k_y a + ik_x a)^2] \end{aligned} \quad (19)$$

Test calculations show that the exact dispersion around \mathbf{K} could be excellently approximated by the above approximation up to $E_C \approx 1.2$ eV, so it is accurate enough for our problem.

In terms of the approximate $\phi(\mathbf{k})$, the velocity vector satisfies $\mathbf{q} \cdot (\mathbf{v}_{\mathbf{k}} + \mathbf{v}_{\mathbf{k}+\mathbf{q}})/2 = \phi(\mathbf{k} + \mathbf{q}) - \phi(\mathbf{k})$. The impurity scattering part of the heat current operator could thus be written as $\frac{1}{V_0} \sum_{\mathbf{q}} V_i(\mathbf{q}) \mathbf{j}_N(\mathbf{q})$.

Since the particle current operator is the same as that without of impurity scattering, the linear response coefficient L_{11} could easily be shown to be[7, 19, 20, 36]

$$\begin{aligned} L_{11} = & T \int_{-\infty}^{+\infty} \frac{d\epsilon}{2\pi} \left[-\frac{\partial n_F(\epsilon)}{\partial \epsilon} \right] \text{Re} \{ P_{11}(\epsilon - i0^+, \epsilon + i0^+) \\ & - P_{11}(\epsilon + i0^+, \epsilon + i0^+) \}. \end{aligned} \quad (20)$$

The kernel is defined as

$$P_{11}(z, z') = \frac{2}{dV_0} \sum_{\mathbf{k}} \text{Tr} \{ G_{\mathbf{k}}(z) \mathbf{\Gamma}_1(\mathbf{k}, z, z') G_{\mathbf{k}}(z') \cdot \mathbf{j}_1^{\mathbf{k}} \}, \quad (21)$$

with $\mathbf{\Gamma}_1(\mathbf{k})$ as the vertex function corresponding to the wave vector \mathbf{k} .

Taking into account of the relationship $\mathbf{j}_1^{\mathbf{k},\mathbf{q}} = \frac{1}{2}\mathbf{j}_1^{\mathbf{k}} + \frac{1}{2}\mathbf{j}_1^{\mathbf{k}+\mathbf{q}}$, and following the same route as for the single orbital model[36], it could be proved that L_{12} could be written into the following form [5, 7, 36]

$$\begin{aligned} L_{12} = & T \int_{-\infty}^{+\infty} \frac{d\epsilon}{2\pi} \left[-\frac{\partial n_F(\epsilon)}{\partial \epsilon} \right] \text{Re} \{ P_{12}(\epsilon - i0^+, \epsilon + i0^+) \\ & - P_{12}(\epsilon + i0^+, \epsilon + i0^+) \}. \end{aligned} \quad (22)$$

The kernel P_{12} is simply P_{11} multiplied by the energy

$$P_{12}(\epsilon \mp i0^+, \epsilon + i0^+) = \epsilon P_{11}(\epsilon \mp i0^+, \epsilon + i0^+). \quad (23)$$

In our calculations, the positive infinitesimal 0^+ would be replaced by a small positive quantity η . In this work, we adopt $\eta=1$ meV. A smaller η is verified not to change the results to be presented in what follows.

Under the SCBA, the 4×4 Green's function matrix is defined as $G_{\mathbf{k}}(z) = (G_{\mathbf{k}}^0(z)^{-1} - \Sigma_{\mathbf{k}}(z))$. The self energy is determined by the following self-consistency relation

$$\Sigma_{\mathbf{k}}(z) = \frac{n_i}{V_0} \sum_{\mathbf{k}'} |v_i(\mathbf{k} - \mathbf{k}')|^2 [G_{\mathbf{k}'}^0(z) - \Sigma_{\mathbf{k}'}(z)]^{-1}, \quad (24)$$

where $G_{\mathbf{k}}^0(z) = [z + \mu - H_0(\mathbf{k})]^{-1}$ is the free Green's function. μ is the chemical potential determined from the free Hamiltonian for a certain carrier density. In this work, we would neglect the shift in μ by the impurity potential. This is known as not giving rise to qualitative changes when the impurity concentration is not very high[7]. After obtaining the Green's functions, the vertex functions are calculated by the following self-consistency relation

$$\mathbf{\Gamma}_1(\mathbf{k}, z, z') = \mathbf{j}_1^{\mathbf{k}} + \frac{n_i}{V_0} \sum_{\mathbf{k}'} |v_i(\mathbf{k} - \mathbf{k}')|^2 G_{\mathbf{k}'}(z) \mathbf{\Gamma}_1(\mathbf{k}', z, z') G_{\mathbf{k}'}(z'). \quad (25)$$

In obtaining the above self-consistent relations, averages over impurity configurations have been done under SCBA as[37]

$$\langle \rho_i(\mathbf{q}) \rho_i(-\mathbf{q}') \rangle = N_i \delta_{\mathbf{q},\mathbf{q}'}, \quad (26)$$

where $N_i = n_i V_0$ is number of impurities in the system under consideration. For a set of \mathbf{k} vectors, we can get

the Green's functions and the vertex functions, then they are used to calculate the kernels P_{11} and P_{12} , and hence the linear response coefficients L_{11} and L_{12} could be obtained. If the full Brillouin zone (BZ) is utilized, the number of wave vectors would be too large for a practical calculation. However, since only intravalley scattering is relevant for charged impurities[7, 15–17], we could focus on the low energy states within a cutoff energy E_C around a single valley.

III. RESULT AND DISCUSSION

To see the effect of impurity scattering more clearly, we first present the results for clean systems, where the bare Green's functions and vertex functions are used. The room temperature (300 K) thermopower of clean monolayer and gapless bilayer graphene are presented in Fig 1(a). Here and later, the abscissa index x represents the electron doping averaged to per site, which could be controlled by an external gate voltage[2–4]. $x=0.001$ amounts to an electron density of $3.82 \times 10^{12} \text{ cm}^{-2}$ per layer. For the monolayer system[42], a tight binding model up to nearest-neighbor hopping $t=3 \text{ eV}$ is used. Peak values of the two curves are almost the same, with that of the monolayer slightly larger. When a more realistic parameter $t=2.7 \text{ eV}$ is used for the monolayer graphene[21], the peak position shifts slightly away from $x=0$, while the peak value keeps almost unchanged as about $\pm 83 \mu\text{V/K}$. Besides the low carrier density peak, thermopower of gapless bilayer graphene shows a second smaller peak at a higher carrier concentration. The onset of the second peak, for which the peak position corresponds to a chemical potential of $|\mu| \simeq 316 \text{ meV}$, is associated with the crossing of the chemical potential with the lower valence band (band top at $-t_{\perp} = -300 \text{ meV}$) or the upper conduction band (band bottom at $t_{\perp} = 300 \text{ meV}$).

We now explore the effect of opening a band gap in the clean bilayer graphene. Figure 1(b) shows the thermopower of bilayer graphene for a series of potential differences V between the two layers. With the increase of V , peak value of the thermopower increases quickly. For $V = 1 \text{ eV}$ (corresponding to an energy gap of approximately 288 meV , which is experimentally achievable[13]), peak value of the thermopower is about $412 \mu\text{V/K}$, which is more than four times that of the value in monolayer graphene and zero gap bilayer graphene. The much smaller second peak shifts continuously to larger x as V increases and becomes irrelevant as V increases to 1 eV . Hence, we would concentrate on the region of low carrier density in the following. The smallest energy gap between the conduction band and the valence band increases with V as $\Delta = \frac{V t_{\perp}}{\sqrt{t_{\perp}^2 + V^2}}$ [22, 43], which is shown as an inset of Fig. 1(b). The large magnitude of thermopower and the tunability of gap make the biased bilayer graphene a more promising candidate for future thermoelectric applications as compared with monolayer graphene.

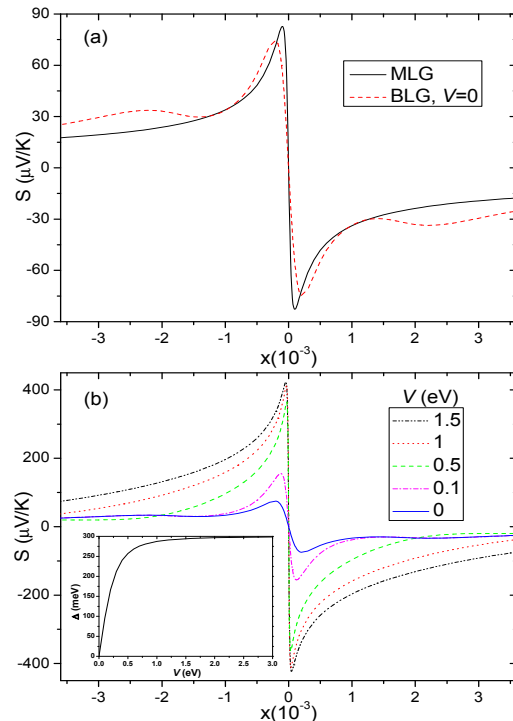


FIG. 1: (a) Room temperature thermopower as a function of carrier density for clean monolayer graphene (MLG) and gapless bilayer graphene (BLG). (b) Room temperature thermopower of BLG for a series of potential energy differences V between the two layers. Inset of (b) shows the evolution of the global energy gap Δ as a function of V .

In the following, we focus on the biased bilayer graphene system with $V=1 \text{ eV}$. In Fig. 2(a), thermopower of this system is shown as a function of chemical potential (μ) for three different temperatures. When μ is at the band edge ($\sim \pm 0.144 \text{ eV}$), thermopower of all three temperatures are nearly identical to each other. When μ is inside of the band gap, $|S|$ increases as temperature decreases. While when μ lies in the bands, $|S|$ increases as temperature increases. This is similar to the corresponding behavior in semiconducting armchair graphene nanoribbons[42, 44]. The corresponding dependence of x on μ is illustrated in Fig. 2(b). When x is very close to zero, $|\mu|$ decreases as temperature increases. As $|x|$ increases beyond a certain critical value, $|\mu|$ increases as temperature increases. The above complex temperature dependence is a direct result of the existence of the band edge Van Hove singularities. From Fig. 2(a) and Fig. 2(b), it is clear that for 100 K , peak value of S is achieved at a doping very close to zero. As temperature increases, the carrier density for the peak increases continuously to larger values.

Now, we begin to study the effect of impurity. In this work, charged impurity is considered as the only source of scattering for impure bilayer graphene. Thermopower of bilayer graphene for a series of different impurity con-

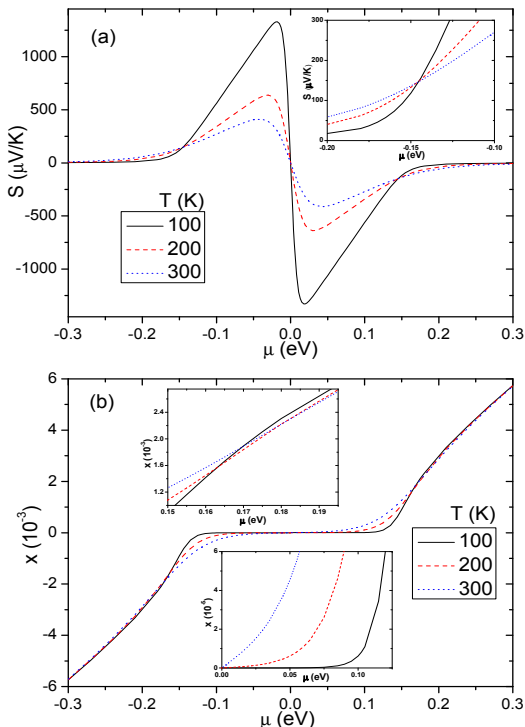


FIG. 2: (a) Thermopower as a function of chemical potential for a biased bilayer graphene, at three different temperatures. (b) The corresponding variation of doping concentration x as a function of the chemical potential. Inset of (a) shows an enlargement of the curves close to the valence band top (~ 0.144 eV). Lower inset of (b) shows an enlargement of the small μ and small x region. Upper inset of (b) shows an enlargement of the region where the temperature dependence of μ for fixed x changes.

centrations are shown in Fig. 3(a), at room temperature for $V = 1$ eV. Curve for clean system is also displayed as a reference. In order to ensure that the SCBA is valid, we consider only cases with small impurity concentrations. Up to a concentration of $n_i = 5 \times 10^{10} \text{ cm}^{-2}$ per layer, peak value of the thermopower increases continuously with the impurity concentration. The peak position remains unchanged. In these relatively clean systems, the influence of localization[22–24] can be safely neglected.

Here and later when impurity scattering is considered, an energy cutoff of $E_C = 0.5$ eV is used. Test calculations by increasing E_C show no perceivable change in the results for both clean and impure systems in the considered low carrier density region. For most energies, the self-consistency for the Green's functions and vertex functions converge within 100 iterations with an accuracy of 10^{-5} and 10^{-4} for the modulus of every element, respectively. For a symmetric band structure, as is the case for both clean monolayer and bilayer graphene, thermopower is an odd function of the carrier density[1, 7]. In the presence of charged impurities, the electron-hole symmetry of the band is preserved which could be seen

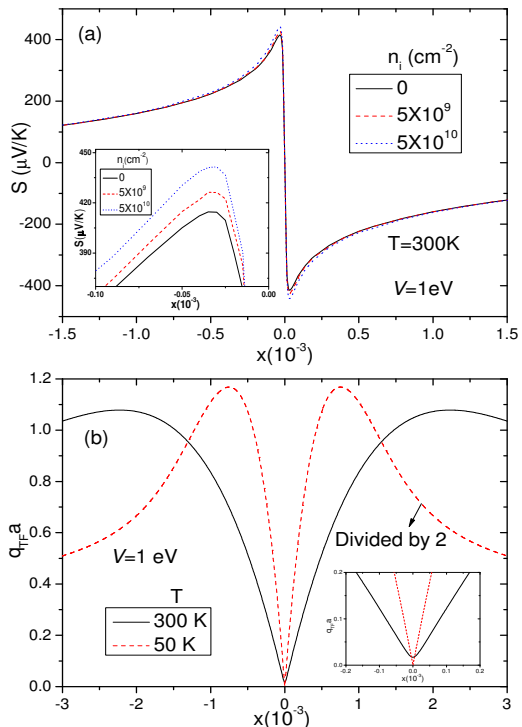


FIG. 3: (a) Room temperature thermopower of bilayer graphene for a series of different impurity concentrations with $V=1$ eV. (b) The Thomas-Fermi screening wave vector at 300 K and 50 K for bilayer graphene with $V=1$ eV. The curve for 50 K is divided by a factor of 2. Insets of (a) and (b) show an enlargement of the corresponding low carrier density parts.

by explicitly calculating the density of states. So we expect the relationship $S(-x) = -S(x)$ survives. The full curve for $n_i = 5 \times 10^{10} \text{ cm}^{-2}$ and $T = 300$ K is calculated explicitly, verifying the above statement. To save computing time, for all other parameter sets in the presence of impurity, thermopower is calculated explicitly for the hole doped cases with $x \leq 0$. The results for $x > 0$ are obtained through $S(x) = -S(-x)$.

The Thomas-Fermi screening wave vector is shown in Fig. 3(b) as a function of carrier density at 300 K and 50 K for $V=1$ eV. At 300 K, as a result of thermal excitations, we get a finite $q_{TF} a \approx 0.017$ for zero doping. As temperature goes down, the zero doping Thomas-Fermi screening wave vector decreases gradually. As could be seen in the inset of Fig. 3(b), $q_{TF}(x=0)$ is very close to zero at 50 K. This result is similar to the monolayer graphene system and is different from the gapless bilayer graphene, for which the zero doping q_{TF} is finite even at zero temperature for the nonvanishing density of states there[45]. The two peaks in Fig. 3(b) arise from the Van Hove singularities near the conduction band bottom and the valence band top, and are shifted to larger carrier densities at higher temperature by thermal excitations.

Previous works[1–4, 7, 42] on monolayer graphene show that impurity scattering is essential to reproduce the tem-

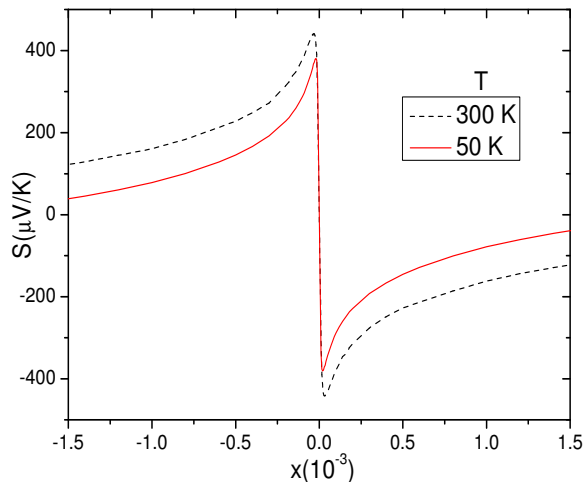


FIG. 4: Thermopower of gapped bilayer graphene at 300 K and 50 K as a function of carrier density, for $V=1$ eV and $n_i=5 \times 10^{10} \text{ cm}^{-2}$.

perature dependence of the thermopower observed experimentally. Thermopower of gapped bilayer graphene with the same impurity concentration $n_i=5 \times 10^{10} \text{ cm}^{-2}$ are shown as a function of carrier density for room temperature and 50 K in Fig. 4. Results for $x \geq 10^{-5}$ are readily obtained for both temperatures. However, for x at and very close to zero, only results for $T=300$ K are obtained within our calculation time. This is understood from Fig. 3(b) as a result of reduced screening at a temperature as low as 50 K[7]. As temperature decreases, thermopower is suppressed and peak position of thermopower shifts slightly towards zero doping. These results are qualitatively very similar to the experimental results for monolayer graphene[2–4].

A peculiar feature of our results is that the maximum value of S at room temperature increases with impurity concentration n_i , as shown in Fig. 3(a). By increasing the energy cutoff E_C and the number of wave vectors in the Brillouin zone, we have verified that the above result is robust. In order to have a better understanding, we show the variation of L_{11} and L_{12} for $x=-3 \times 10^{-5}$ in Fig. 5(a). It is clear that, both L_{11} and L_{12} decrease sharply as n_i increases. However, the reduction of L_{11} is somewhat larger than that of L_{12} . The increase of room temperature S thus comes as a result of the stronger dependence of L_{11} on n_i as compared with L_{12} . The reason why L_{11} decreases faster than L_{12} as n_i increases is encoded in the integration kernels of the two linear response coefficients, Eq. (21) and Eq. (23). Eq. (23) shows that states above and below of the chemical potential contribute to L_{12} in opposite sign but of the same sign for L_{11} . Hence L_{11} is more sensitive to the variation of density of states (DOS) in the conduction band and

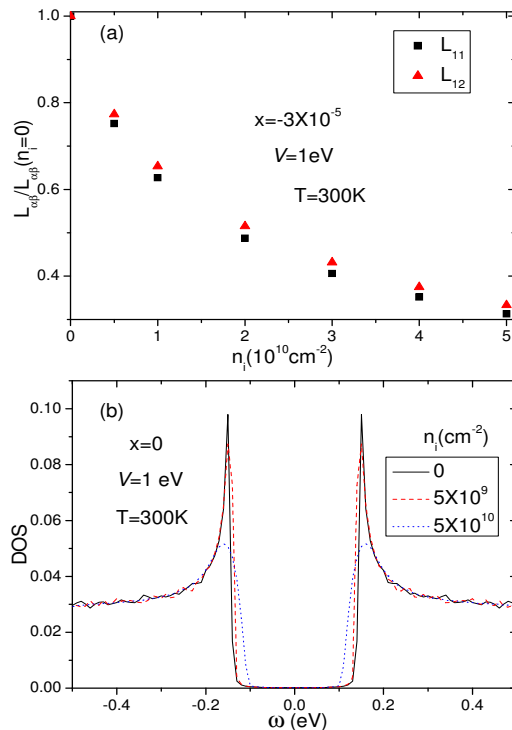


FIG. 5: (a) Variation of L_{11} and L_{12} as a function of impurity concentration for $x=-3 \times 10^{-5}$, normalized by the $n_i=0$ value, respectively. (b) Low energy density of states (DOS) for three different impurity concentrations.

valence band due to the presence of impurities which is shown in Fig. 5(b) for two impurity concentrations at $V=1$ eV and $T=300$ K. In a previous theoretical work on graphene nanoribbon[42], a similar increase of S with defect density is also observed.

We now try to understand the doping dependence of the shape of thermopower in the small carrier density region. From the definitions in Eqs. (16), (20) and (22), thermopower could be understood as the average value of $(E - \mu)$ weighted by the combination of electron group velocity (encoded in $\mathbf{v}_{\mathbf{k}}$ in the current operator and the renormalized current vertex) and DOS [42, 46]. States above and below of the chemical potential contribute in the opposite sign to S . At the same time, the factor $\partial n_F / \partial \omega = -n_F(1 - n_F) / k_B T$ is substantially nonzero only in an energy range of several $k_B T$ centered symmetrically around the chemical potential. It is thus easy to understand that S tends to be larger once the DOS and (or) group velocity between states above and below the chemical potential have a big contrast[47]. According to this picture, when μ is deep inside of the band (but still in the low carrier density region), where the DOS is nearly flat according to Fig. 5(b), the thermopower would be small. As the chemical potential moves close to the band edge, difference between states above and below of the chemical potential increases, which results in the increase of S . At finite temperature, when the doping is at or very

close to the band edge Van Hove singularities, μ would be inside of the gap. In these cases, all states are high energy states measured from μ . Since S would be larger once the higher $|E - \mu|$ states contribute more to the integration, S is expected to continue increase for very low carrier densities. As shown in previous works[42, 46], for μ inside of the semiconducting gap, the most significant part of S comes from a term of the form

$$S \sim \left(\frac{\Delta}{2} - |\mu|\right)/eT, \quad (27)$$

which clearly shows the increase of S as $\mu \rightarrow 0$ (or equivalently, $x \rightarrow 0$).

The above picture explains the initial increase of thermopower as $|x|$ decreases. However, when the carrier density is very close to zero, the chemical potential also lies close to zero energy. Hence, both the valence band and the conduction band states are present by thermal excitations. Since the contributions to thermopower from valence and conduction band states are opposite in sign, the thermopower is expected to decrease at a critical carrier density characterized by the temperature[2, 3, 42]. The critical $|x|$ below which the magnitude of thermopower starts to decrease is thus expected to increase with temperature. This explains the shift of peak position as observed in Fig. 2 and Fig. 4. In Ref. 7 on thermopower of monolayer graphene, the deviation at low carrier density from the higher density Mott's behavior [1, 46] is ascribed to impurity scattering mediated coherence between the conduction and valence bands. According to this mechanism, as impurity concentration n_i increases, the above coherence effect should enhance. So a shift of peak position with n_i is expected. At 50 K and for $n_i = 5 \times 10^{10} \text{ cm}^{-2}$, the peak position is shown to shift from $x_C \simeq 0$ to $x_C \simeq 2 \times 10^{-5}$. However, for 300 K, the x_C show no perceivable variation with n_i up to $n_i = 5 \times 10^{10} \text{ cm}^{-2}$. A calculation beyond the SCBA is needed to know whether or not the peak position for 300 K would shift for much larger n_i .

It is also interesting to ask why introducing a gap significantly enhances the thermopower of bilayer graphene. Formerly, a 'pudding mold' mechanism[47] is introduced to account for the large thermopower observed in Cobaltates. In that model, a band with a somewhat flat portion connected to a highly dispersive portion is proposed to give high thermopower when the chemical potential lies close to the bending point. Band structure of biased bilayer graphene is exactly of 'pudding mold' like[9, 47]. So the increase of S with V for a carrier density typically of $x = \pm 0.001$, for which the chemical potential lies inside of the band, is understood as resulting from the onset of the 'pudding mold' mechanism. However, peak value of S occurs when μ situates inside of the band gap. In this case, as mentioned above, S_{max} could be estimated by Eq. (27)[42, 46]. For $V = 1 \text{ eV}$, $\Delta \simeq 288 \text{ meV}$. For $x = -3 \times 10^{-5}$ and $T = 300 \text{ K}$, the chemical potential $\mu \simeq -40 \text{ meV}$, Eq. (27) gives a value of approximately $347 \mu\text{V/K}$ which is about 80 percent of the values in Fig. 2(a). So in

the present case, S_{max} is set by the energy gap Δ , which increases with V and is bounded by a limit, t_{\perp} [22, 43]. Hence, the large maximum thermopower in biased bilayer graphene is mainly a result of the energy gap.

Taking into account of the band asymmetry arising from the on-site energy difference between the two kinds of carbon sublattices, the band gap becomes asymmetric and the conduction (or the valence, depending on the sign of V) band would be more flat[48]. However, since the on-site energy difference derived from experiment is only about 0.018 eV [48], we expect the above effect is extremely small and would not change our present result much. The interlayer hopping is estimated to be in the range of $t_{\perp} \sim 0.3 - 0.4 \text{ eV}$ [49]. Our test calculation in clean system with $t_{\perp} = 0.4 \text{ eV}$ for $V = 1 \text{ eV}$ (with other parameters unchanged) gives a peak thermopower value of approximately $544 \mu\text{V/K}$ at 300 K, which is $132 \mu\text{V/K}$ larger than the result for $t_{\perp} = 0.3 \text{ eV}$. So, the thermopower of gapped bilayer graphene is large regardless of the choice of model parameters.

Applying an electric field to trilayer or other multilayer graphene system, a gap could also be induced[30, 31]. For certain parameters, the band structure is also of 'pudding mold' like[30, 31]. It is thus interesting to ask how the peak value of thermopower evolves as a function of the layer number. In this work, we have only considered the effect of charged impurity scatterings. Recently, it has been proposed that scattering by short-range disorder may also play an important role in the transport of gapless bilayer graphene because the screening of charged impurities in zero gap bilayer graphene is much stronger than that in monolayer graphene[18, 45]. Though we believe that the degree of screening in gapped bilayer graphene should be much smaller than that in the gapless system, it is an interesting question whether the inclusion of short-range scatterers would change our present results much. On the other hand, the regime of large impurity concentration or strong impurity strength deserves an explicit study in terms of a less severe approximation as compared with SCBA used above. We defer the above questions to later studies.

IV. SUMMARY

We have theoretically studied the thermopower of bilayer graphene. If a band gap of approximately 288 meV is induced in the system by an external bias, the room temperature thermopower is greatly enhanced by a factor of larger than 4 as compared with that of the monolayer graphene and the gapless bilayer graphene. In the presence of dilute charged impurities, peak value of the room temperature thermopower is shown to increase slightly. This behavior is analyzed in terms of the different dependence of L_{11} and L_{12} on the modification of density of states by impurity. As temperature decreases, peak position of thermopower shifts slightly towards zero carrier density in the presence of dilute charged impurities.

Acknowledgments

We wish to acknowledge the support of NSC 98-2112-M-001-017-MY3. Part of the calculations was performed

in the National Center for High-Performance Computing in Taiwan.

-
- [1] E. H. Hwang, E. Rossi, and S. Das Sarma, Phys. Rev. B **80**, 235415 (2009).
- [2] Yuri M. Zuev, Willy Chang, and Philip Kim, Phys. Rev. Lett. **102**, 096807 (2009).
- [3] Peng Wei, Wenzhong Bao, Yong Pu, Chun Ning Lau, and Jing Shi, Phys. Rev. Lett. **102**, 166808 (2009).
- [4] Joseph G. Checkelsky and N. P. Ong, Phys. Rev. B **80**, 081413(R) (2009).
- [5] Thomas Löfwander and Mikael Fogelström, Phys. Rev. B **76**, 193401 (2007).
- [6] Balázs Dóra and Peter Thalmeier, Phys. Rev. B **76**, 035402 (2007).
- [7] Xin-Zhong Yan, Yousef Romiah, and C. S. Ting, Phys. Rev. B **80**, 165423 (2009).
- [8] Lijun Zhu, R. Ma, L. Sheng, M. Liu, and D. N. Sheng, Phys. Rev. Lett. **104**, 076804 (2010).
- [9] Edward McCann, Phys. Rev. B **74**, 161403(R) (2006).
- [10] Hongki Min, Bhagawan Sahu, Sanjay K. Banerjee, and A. H. MacDonald, Phys. Rev. B **75**, 155115 (2007).
- [11] Eduardo V. Castro, K. S. Novoselov, S. V. Morozov, N. M. R. Peres, J. M. B. Lopes dos Santos, Johan Nilsson, F. Guinea, A. K. Geim, and A. H. Castro Neto, Phys. Rev. Lett. **99**, 216802 (2007).
- [12] Jeroen B. Oostinga, Hubert B. Heersche, Xinglan Liu, Alberto F. Morpurgo, and Lieven M. K. Vandersypen, Nature Materials **7**, 151 (2008).
- [13] Yuanbo Zhang, Tsung-Ta Tang, Caglar Girit, Zhao Hao, Michael C. Martin, Alex Zettl, Michael F. Crommie, Y. Ron Shen, and Feng Wang, Nature **459**, 820 (2009).
- [14] Kin Fai Mak, Chun Hung Lui, Jie Shan, and Tony F. Heinz, Phys. Rev. Lett. **102**, 256405 (2009).
- [15] Kentaro Nomura and A. H. MacDonald, Phys. Rev. Lett. **98**, 076602 (2007).
- [16] E. H. Hwang, S. Adam, and S. Das Sarma, Phys. Rev. Lett. **98**, 186806 (2007).
- [17] Shaffique Adam, E. H. Hwang, V. M. Galitski, and S. Das Sarma, Proc. Natl. Acad. Sci. U. S. A. **104**, 18392 (2007).
- [18] Shudong Xiao, Jian-Hao Chen, Shaffique Adam, Ellen D. Williams, and Michael S. Fuhrer, arXiv:0908.1329v1.
- [19] Nguyen Hong Shon and Tsuneya Ando, J. Phys. Soc. Jpn. **67**, 2421 (1998).
- [20] Xin-Zhong Yan, Yousef Romiah, and C. S. Ting, Phys. Rev. B **77**, 125409 (2008); Xin-Zhong Yan and C. S. Ting, Phys. Rev. B **80**, 155423 (2009).
- [21] N. M. R. Peres, F. Guinea, and A. H. Castro Neto, Phys. Rev. B **73**, 125411 (2006).
- [22] Johan Nilsson and A. H. Castro Neto, Phys. Rev. Lett. **98**, 126801 (2007).
- [23] Mikito Koshino, Phys. Rev. B **78**, 155411 (2008).
- [24] V. V. Mkhitaryan and M. E. Raikh, Phys. Rev. B **78**, 195409 (2008).
- [25] F. Guinea, A. H. Castro Neto, and N. M. R. Peres, Phys. Rev. B **73**, 245426 (2006).
- [26] Johan Nilsson, A. H. Castro Neto, F. Guinea, and N. M. R. Peres, Phys. Rev. B **78**, 045405 (2008).
- [27] Chuanwei Zhang, Sumanta Tewari, and S. Das Sarma, Phys. Rev. B **79**, 245424 (2009).
- [28] Lei Hao, L. Sheng, Solid State Commun. **149**, 1962 (2009).
- [29] Tsuneya Ando, J. Phys. Soc. Jpn. **75**, 074716 (2006).
- [30] A. A. Avetisyan, B. Partoens, and F. M. Peeters, Phys. Rev. B **79**, 035421 (2009).
- [31] Mikito Koshino, arXiv: 0911.3484v1.
- [32] Mikito Koshino and Tsuneya Ando, Phys. Rev. B **73**, 245403 (2006).
- [33] E. H. Hwang and S. Das Sarma, Phys. Rev. B **75**, 205418 (2007).
- [34] Vinay Ambegaokar and Allan Griffin, Phys. Rev. (137), A1151 (1965).
- [35] Adam C. Durst and Patrick A. Lee, Phys. Rev. B **62**, 1270 (2000).
- [36] M. Jonson and G. D. Mahan, Phys. Rev. B **21**, 4223 (1980).
- [37] Gerald D. Mahan, *Many-Particle Physics* (Plenum, New York, 1990) 2nd Ed. Chap. 3 and Chap. 7.
- [38] P. A. Lee, Phys. Rev. Lett. **71**, 1887 (1993).
- [39] Herbert B. Callen, *Thermodynamics and an Introduction to Thermostatistics* (John Wiley & Sons, New York, 1985) 2nd Ed. Chap. 14.
- [40] S. Maekawa, T. Tohyama, S. E. Barnes, S. Ishihara, W. Koshibae, and G. Khaliullin, *Physics of Transition Metal Oxides* (Springer series in solid state sciences, Vol. 144, Springer-Verlag Berlin Heidelberg 2004) Chap. 6.
- [41] P. M. Ostrovsky, I. V. Gornyi, and A. D. Mirlin, Phys. Rev. B **74**, 235443 (2006).
- [42] Yijian Ouyang and Jing Guo, Appl. Phys. Lett. **94**, 263107 (2009).
- [43] Hari P. Dahal, A. V. Balatsky, and Jian-Xin Zhu, Phys. Rev. B **77**, 115114 (2008).
- [44] Yanxia Xing, Qing-feng Sun, and Jian Wang, Phys. Rev. B **80**, 235411 (2009).
- [45] S. Das Sarma, E. H. Hwang, and E. Rossi, arXiv: 0912.0403v1.
- [46] Melvin Cutler and N. F. Mott, Phys. Rev. **181**, 1336 (1969).
- [47] Kazuhiko Kuroki and Ryotaro Arita, J. Phys. Soc. Jpn. **76**, 083707 (2007); R. Arita, K. Kuroki, K. Held, A. V. Lukoyanov, S. Skornyakov, and V. I. Anisimov, Phys. Rev. B **78**, 115121 (2008).
- [48] Z. Q. Li, E. A. Henriksen, Z. Jiang, Z. Hao, M. C. Martin, P. Kim, H. L. Stormer, and D. N. Basov, Phys. Rev. Lett. **102**, 037403 (2009).
- [49] J. W. McClure, Phys. Rev. **108**, 612 (1957); J. C. Slonczewski and P. R. Weiss, Phys. Rev. **109**, 272 (1958).